Received: 26 November 2021 | Accepted: 30 May 2022

DOI: 10.1111/2041-210X.13947

Methods in Ecology and Evolution BRITISH ECOLOGICAL SOCIETY

REVIEW

A review of movement models in open population capture–recapture

Murray G. Efford | Matthew R. Schofield

Department of Mathematics and Statistics, University of Otago, Dunedin, New Zealand

Correspondence
Murray G. Efford
Email: murray.efford@otago.ac.nz

Handling Editor: Torbjørn Ergon

Abstract

1. Understanding rates of survival and recruitment is critical to population management, and capture–recapture methods of estimation are widely used. Spatial models allow for a spatial detection process and can include the movement of activity centres between sampling times. Movement is often treated as a random walk with the step length governed by a probability kernel. However, the movement component of open population spatially explicit capture–recapture models (open SECR) has evolved haphazardly and comparison among studies is difficult.
2. We review published studies, document suitable probability kernels and address the issues of scale and buffer dependence in open SECR by a combination of simulation and case studies on ovenbirds *Seiurus aurocapilla* and tigers *Panthera tigris*.
3. Flexible 2-parameter kernels, such as the bivariate *t*-distribution, fit better than the popular bivariate normal and resulted in higher estimates of survival. We reconcile different parameterizations of the bivariate *t*-distribution and identify a problem when the kernel is defined in terms of its margins.
4. Movement models failed to separate mortality and emigration in simulated data when the data were a random mixture of long and short movements. Our estimates of ovenbird survival were buffer-dependent, and we interpret this as a sign that the data are inadequate for joint modelling of survival and movement. Estimates of tiger survival were more nearly asymptotic on buffer width.
5. We repeat the warning of earlier authors that movement models are effective for separating mortality and emigration only when the data span the range of movement. We appeal for more complete and consistent reporting of movement models and identify topics for future research.

KEYWORDS
activity centre, buffer dependence, dispersal, emigration, mortality, movement kernel, SECR, spatial capture–recapture

1 | INTRODUCTION

Understanding rates of survival and recruitment is critical to population management. Survival and recruitment are increasingly estimated with models that fall under the heading 'open population spatially explicit capture–recapture' (open SECR). These combine conventional capture–recapture methods for survival and recruitment with a spatial model of the detection process: the detection of each individual is most likely when the detector (e.g., trap, hair snag or camera) is near its 'activity centre'. Activity centres are usually not observed directly, but appear in the model as latent variables. When fitting with maximum likelihood, these variables are marginalized (integrated out). When fitting the model within a Bayesian approach using Markov chain Monte Carlo (MCMC), it is common to include the latent variables in the model.

Activity centres are stationary in closed population SECR (Borchers & Efford, 2008; Royle et al., 2014). In reality, individuals may shift their home range over time, leading to dispersal from the natal site, incomplete fidelity to breeding sites, and many other phenomena (e.g., Clobert et al., 2001). Movement between discrete habitat patches may be described by multistate capture–recapture models (Lebreton et al., 2009), and temporary absence from a single patch is considered in non-spatial robust-design models (Kendall et al., 1997). Open SECR enables the modelling of movement processes in continuous space. Capture–recapture datasets are limited in their power to resolve such processes because the observations of each individual are temporally incomplete, but even a simple movement model can be informative and relieve other lack of fit. Open SECR models therefore generally include a simple sub-model for net displacement between sampling times that is the subject of our review.

Capture–recapture estimates of survival may be depressed by unmodelled movement of activity centres between sampling times (we focus here on survival, but per capita recruitment is subject to equivalent and complementary effects). Open SECR has the potential to solve this problem: data simulated with random-walk movement have been found to yield unbiased estimates of survival when the fitted model also includes movement (Efford & Schofield, 2020; Ergon & Gardner, 2014; Gardner et al., 2018; Glennie et al., 2019; Schaub & Royle, 2014). It is therefore tempting to see movement modelling in open SECR as an answer to the longstanding challenge of separating mortality from emigration, or 'true' survival from 'apparent' survival (e.g., Lebreton et al., 1992). A good model for movement will account for survivors that emigrate and thereby eliminate confounding (Ergon & Gardner, 2014; Gardner et al., 2018; Gilroy et al., 2012; Paquet et al., 2020; Schaub & Royle, 2014). This presumes that the data are sufficient to choose a good model and to estimate its parameters.

There are several approaches for including the movement of activity centres in open SECR models, and some notable difficulties. The seminal papers of Ergon and Gardner (2014) and Schaub and Royle (2014) considered a variety of shapes for the movement kernel as we discuss later, but most others have relied on a bivariate normal model (BVN). Random walk movement was modified in several Scandinavian studies by allowing local habitat variables to affect settlement (e.g., Bischof et al., 2020; Milleret et al., 2021). The effect of this modification on modelled patterns of movement has not been explored and we do not consider it here, except to note that restricting settlement to mapped habitat patches is a limiting case (e.g., Reidy et al., 2018). Schaub and Royle (2014) addressed a scenario in which activity centres (nests or territories) were located without error, and hence, there was no need for a spatial detection model (see Reidy et al. (2018) and Paquet et al. (2020) for applications). We include these studies because their movement sub-models are shared with open SECR.

Alternatives to BVN, including bivariate *t* and exponential distributions of distance moved, have been preferred by some authors for the a priori reason that their heavier tails allow an increased probability of long-distance movement, and this reasoning has received quantitative support. Movements by golden-cheeked warblers were modelled more closely by a marginal *t* distribution than either BVN or exponential kernels (Reidy et al., 2018). A bivariate exponential (Laplace) kernel (BVE) provided substantially better model fit (lower AIC) to brushtail possum trapping data than a BVN kernel, although estimates of survival were similar (Efford & Schofield, 2020).

Several authors have noted problems in fitting movement models to open SECR data or pre-empted problems by applying constraints. Gardner et al. (2018) could not estimate the scale parameter of a BVN kernel for the tiger dataset of Karanth et al. (2006). Paquet et al. (2020) fixed the shape parameter of the marginal *t* distribution of movements 'for convergence/identifiability reasons'. Augustine et al. (2020) used a kernel-free approach for capercaillie *Tetrao urogallus* that we discuss later. Others have fitted open SECR models with static activity centres (Chandler et al., 2018; Chandler & Clark, 2014; Gardner et al., 2010; Whittington & Sawaya, 2015).

Table 1 lists published applications of open SECR that have included a model for the movement of activity centres in two dimensions. Further details on the scale of sampling and estimates of movement are given in Appendix S2. Movement has also been included in capture–recapture models for species in one-dimensional habitats such as streams (Fujiwara et al., 2006; Honeycutt et al., 2019; Raabe et al., 2014), but the issues are somewhat different and for simplicity, we do not consider these studies further.

The usual closed SECR model places an array of detectors within a region of habitat (the 'habitat mask' or 'state space') that extends an arbitrary buffer distance from the outermost detectors (natural boundaries are used if convenient). The buffer is chosen to be wide enough that individuals outside the buffer have negligible probability of detection: neither the maximized log likelihood nor the estimates of density change if the buffer is further enlarged, and these quantities become 'buffer independent'.

Movement expands the region from which individuals may be detected over the course of an open SECR study, so a larger buffer is required. Gardner et al. (2018) addressed buffer width in open SECR for the particular case that the population occupies an unknown region near the detectors. However, there has been no general

TABLE 1 Published open SECR models fitted by MCMC ('Bayes') or by maximizing the likelihood ('ML') with various movement models. Parameters of interest: ϕ survival, f per capita recruitment, and D population density. Spatial detection was modelled with a half-normal ('HN') or variable-power ('HVP') function of distance or omitted from model ('None'). Movement kernels: BVN bivariate normal; BVE bivariate Laplace; 2exp marginal exponential; 2t marginal t; RDE radial distance exponential. * indicates settlement modified by habitat covariate. Boundary of the state space was either undefined ('None'), fixed by natural boundaries ('Habitat') or buffered around detectors by a multiple of the half-normal detection scale σ († indicates natural boundary in part). See Appendix S1 for scientific names

				Movement		
Species	Method	Parameter	Detection	Kernel	Boundary	Note
Red-backed shrike	Bayes	ϕ	None	BVN, 2t	None	nest search; 2t $df \geq 2$ [1]
Field vole	Bayes	ϕ	HVP	Various	None	Ugglan traps [2]
Red-backed salamander	Bayes	ϕ	HN	RDE	5 m, 3–8σ	artificial cover objects [3]
Bottle-nosed dolphin	Bayes	ϕ	HVP	RDE	Habitat	photo-identification [4]
Tiger	Bayes	ϕ, D	HN	BVN	10–18 km, 5–9σ	automatic cameras [5]
Golden-cheeked warbler	Bayes	ϕ	None	BVN, 2exp, 2t	None	territory search, disjunct habitat [6]
Ocelot	Bayes	ϕ, f, λ	HN	BVN	3σ	automatic cameras [7]
Jaguar	ML	ϕ, D	HN	BVN	17 km, 6σ	automatic cameras [8]
Brushtail possum	ML	ϕ, D	HN	BVN, BVE	200 m, 6σ †	cage traps; kernel truncated [9]
Northern wheatear	Bayes	ϕ	None	2t*	None	territory search; 2t $df = 5$ [10]
Brown bear	Bayes	ϕ, D	HN	BVN*	40 km, 4.5–7σ †	DNA multiple sources [11,12]
Wolf	Bayes	ϕ, D	HN	BVN*	40 km, 5σ †	DNA multiple sources [12]
Wolverine	Bayes	ϕ, D	HN	BVN*	60 km, 6–8σ †	DNA multiple sources [12, 13, 14]

Notes: [1] Schaub & Royle, 2014, [2] Ergon & Gardner, 2014, [3] Muñoz et al., 2016, [4] McDonald et al., 2017, [5] Gardner et al., 2018, [6] Reidy et al., 2018, [7] Satter et al., 2019, [8] Glennie et al., 2019, [9] Efford & Schofield, 2020, [10] Paquet et al., 2020, [11] Bischof et al., 2016, [12] Bischof et al., 2020, [13] Milleret et al., 2020, [14] Milleret et al., 2021.

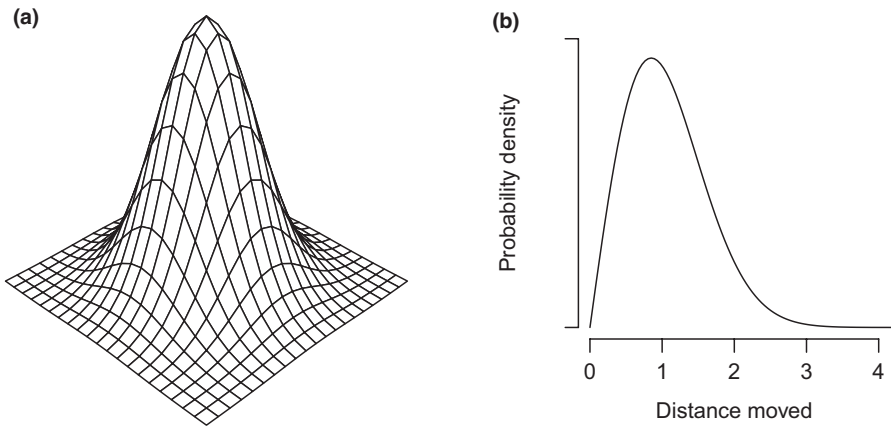

FIGURE 1 Schematic (a) 2-dimensional movement kernel $g(r)$ centred on initial location, and (b) corresponding distribution of distance moved $f(r)$, where r is distance from initial location. Possible functions $f(r)$ are listed in Table 2.

consideration of buffer dependence in unbounded habitat and the effect of kernel choice.

Our goal in this paper is to review the state of the art and to clarify some limitations of open SECR models. We focus on three aspects: (a) the choice of movement kernel, (b) the effect that the scale of sampling has on the estimation of movement and survival and (c) the impact of buffer width on estimation of movement and survival. These issues are explored by simulation and through the application of open SECR to two field datasets. The first is a small dataset from mistnetting of ovenbirds *Seiurus aurocapilla* over 5 breeding seasons in Maryland, USA, and the second is a larger dataset from a 10-year camera study of tigers *Panthera tigris* in India (Karanth et al., 2006).

2 | MOVEMENT KERNELS

In this section, we detail the available movement kernels and their properties, while attempting to clarify some technical and terminological issues. The movement kernel can be defined in either Cartesian or polar space. A kernel defined in Cartesian space is a

TABLE 2 Continuous bivariate kernel models expressed as function of radial distance r. Distribution of distance moved is given by the probability density function $f(r)$ and cumulative probability $F(r)$. BVN, BVE, BVT and BVC are 'native' circular bivariate distributions ($g(r) = f(r) / (2\pi r)$), whereas RDE, RDG and RDL combine a univariate distribution $f(r)$ with a circular-uniform direction θ (i.e. using polar coordinates)

Kernel	Alias	$f(r)$	Mean	Median	$F(r)$
Exponential	RDE	$\frac{1}{\alpha}\exp\left(\frac{-r}{\alpha}\right)$	α	$\alpha\ln(2)$	$1-\exp\left(\frac{-r}{\alpha}\right)$
Gamma	RDG	$\frac{1}{\Gamma(\beta)\alpha^{\beta}}r^{\beta-1}\exp\left(\frac{-r}{\alpha}\right)$	$\alpha\beta$	no simple form	$\frac{1}{\Gamma(\beta)}\gamma\left(\beta,\frac{r}{\alpha}\right)$
Lognormal	RDL	$\frac{1}{r\sigma\sqrt{2\pi}}\exp\left(\frac{-(\ln(r)-\mu)^2}{2\sigma^2}\right)$	$\exp\left(\mu+\frac{\sigma^2}{2}\right)$	$\alpha=\exp(\mu)$	$\Phi\left(\frac{\ln(r)-\mu}{\sigma}\right)$
Bivariate normal	BVN	$\frac{r}{\alpha^2}\exp\left(\frac{-r^2}{2\alpha^2}\right)$	$\sqrt{\frac{\pi}{2}}\alpha$	$\sqrt{2\ln(2)\alpha^2}$	$1-\exp\left(\frac{-r^2}{2\alpha^2}\right)$
Bivariate Laplace	BVE	$\frac{r}{\alpha^2}\exp\left(\frac{-r}{\alpha}\right)$	2α	no simple form	$1-\left(\frac{r}{\alpha}+1\right)\exp\left(\frac{-r}{\alpha}\right)$
Bivariate t	BVT	$\frac{2\beta r}{\alpha^2}\left(1+\frac{r^2}{\alpha^2}\right)^{-(\beta+1)}$	$\alpha\frac{\sqrt{\pi}}{2}\frac{\Gamma(\beta-0.5)}{\Gamma(\beta)}$, $\beta>0.5$	$\alpha\sqrt{2^{\frac{1}{\beta}}-1}$	$1-\left(\frac{\alpha^2}{\alpha^2+r^2}\right)^{\beta}$
Bivariate Cauchy	BVC	$\frac{r\alpha}{(\alpha^2+r^2)^{\frac{3}{2}}}$	undefined	$\alpha\sqrt{3}$	$1-\frac{\alpha}{\sqrt{\alpha^2+r^2}}$

Note: γ is the lower incomplete gamma function and Φ is the standard normal distribution function.

2-dimensional probability density for the final x and y coordinates of an individual initially at the origin. A kernel defined in polar space is the joint probability density of direction and radial distance; we generally assume that these are independent and that the distribution of direction is uniform.

The probability density in Cartesian space is denoted $g(x,y)$. If this density can be defined completely by the radial distance $r=\sqrt{x^2+y^2}$, we refer to it as $g(r)$, notation consistent with that used in plant dispersal modelling (e.g., Cousens et al., 2008). It is straightforward to move from the 2-dimensional density $g(r)$ to the univariate density of radial distance that we denote as $f(r)=2\pi r g(r)$. The intuitive explanation for the relationship is that we must account for increasing circumference with increasing radius. The distinction between $g(r)$ and $f(r)$ is important: the density $g(r)$ is a bivariate density defined in Cartesian space, while $f(r)$ is a univariate density defined in polar space. For example, a bivariate normal kernel $g(r)$ has a mode at $r=0$, while the corresponding univariate density $f(r)$ is positive and skewed, with mode >0 (Figure 1). In Appendix S3, we provide more formal notation that makes explicit the use of Cartesian or polar space and allows a density transformation between these spaces in the general case.

2.1 | Survey of kernel functions

We consider kernels in two groups. Kernels in the first group are defined in polar space, through $f(r)$ (Ergon & Gardner, 2014). We distinguish these with the prefix RD (radial distance). Kernels in the second group are defined in Cartesian space in terms of the bivariate distribution $g(r)$, from which $f(r)$ is derived secondarily (Efford & Schofield, 2020). For these, we use the prefix BV (bivariate).

Kernels are listed in Table 2, each with its mean, median and cumulative distribution function $F(r)$. Each has a scale parameter and three (RDG, RDL and BVT) have an additional parameter that varies the shape of the distribution. We use α for the scale and β for the shape parameter across all distributions. The lognormal distribution is usually parameterized in terms of the mean μ and SD σ of the log values; we suggest using the median $\exp(\mu)$ as the scale parameter α, and $\beta=1/\mathrm{CV}^2(r)=1/\left(e^{\sigma^2}-1\right)$ as a convenient shape parameter that is independent of scale. Some kernels arise as special cases of others; for example, exponential distance moved RDE corresponds to gamma distance moved RDG with shape parameter $\beta=1$. We next comment specifically on the bivariate kernels not considered by Ergon and Gardner (2014).

2.2 | Bivariate normal kernel, BVN

The circular bivariate normal (BVN or Gaussian) kernel was the first to be suggested for open SECR (Gardner et al., 2010) and has been used widely (Table 1). The BVN kernel has some useful properties not shared by other kernels, particularly that cumulative movement over k sessions is equivalent to single-step movement with an inflated kernel whose scale parameter is $k\alpha^2$ (Glennie et al., 2019). This enables a simple adjustment for varying sampling interval when α is constant in time. However, the BVN kernel has a major shortcoming as a description of biological dispersal: the corresponding distribution of dispersal distances has a light tail ($f(r)$ approaches zero rapidly for large r), whereas dispersal processes in general have heavy tails (e.g., Nathan et al., 2012). One consequence of the light tail is that occasional long movements will have a disproportionate effect on the fitted scale parameter. The probability density of distance moved has a Weibull distribution with shape parameter 2 and scale $\sqrt{2}\alpha$, otherwise known as a Rayleigh distribution.

2.3 | Bivariate laplace kernel, BVE

A circular bivariate negative exponential (BVE or Laplace) kernel was used by Efford and Schofield (2020) and has a single parameter that determines the scale of movement, but its tail is markedly heavier

than BVN. The negative exponential form used here and elsewhere in ecology to define the BVE (e.g., Clark et al. (1999, Eq 5a), Cousens et al. (2008, Table 5.2), Nathan et al. (2012, Table 15.1)) is not the bivariate symmetric Laplace distribution considered by Kotz et al. (2001, p. 231), defined in terms of Bessel functions and with infinite density at $r = 0$. The bivariate Laplace kernel corresponds to RDG with $\beta = 2$.

2.4 | Bivariate *t* distribution kernel, BVT

The univariate *t*-distribution has a heavier tail than the exponential for small degrees of freedom ν, and is an obvious choice for dispersal modelling. A bivariate *t* distribution (BVT) was described for seed dispersal by Clark et al. (1999). The shape of the BVT kernel varies with the degrees of freedom. For large degrees of freedom the shape approaches BVN, and for $\nu = 1$ ($\beta = 0.5$) the distribution is bivariate Cauchy (BVC). The mean of the distribution is undefined for $\nu \leq 1$ ($\beta \leq 0.5$). Parameterizations of the BVT differ in notation and scaling of the shape parameter (Appendix S4).

Van Houtan et al. (2007) and others have modelled bird dispersal with a 2-parameter log-hyperbolic secant (log-sech) kernel that closely matches BVT in shape (unpublished results) and also has the bivariate Cauchy as a special case. Other properties of the log-sech distribution are not well documented and we do not consider it further.

2.5 | Marginal specification

The kernels in Table 2 are all defined as a function of distance r. In Cartesian space, their contours of probability are circular; in polar space the movement angle θ and radial distance r are independent, and θ has uniform density over $[0,2\pi)$. Another way to specify a kernel is to treat the Cartesian coordinates x and y as varying independently according to some shared univariate marginal distribution. When each coordinate follows the same normal (Gaussian) distribution, their joint distribution is BVN, the circular bivariate normal. However, combining independent non-Gaussian marginal distributions, such as Student's *t* or Laplacian, results in a bivariate distribution with non-circular contours of probability (e.g., Appendix S4, Figure S1). In polar space, this leads to a lack of independence between θ and r, and in most cases to non-uniform densities for θ. This is inelegant as it introduces potential confounding with the orientation of habitat features or the detector array.

A marginal specification has been used in several studies for non-Gaussian distributions, particularly the *t* distribution (Table 1). The bivariate distribution with *t*-distributed margins is especially non-circular for small degrees of freedom. Further analytical evaluation is possible for marginal Laplace densities (Appendix S4). For example, the density of θ is quadrimodal and the expected distance $E[r] \approx 1.6232\alpha$, compared to $E[r] = 2\alpha$ for the bivariate Laplace distribution in Table 2.

2.6 | Zero-inflated kernels

Other kernels may be devised as probabilistic mixtures of distributions such as those in Table 2. Zero-inflated distributions $f_z(r)$ allow some individuals to move in a particular interval according to a standard kernel while others do not move at all. The possibility that dispersal and philopatry are categorically different behaviours lends this some appeal. Ergon and Gardner (2014) fitted zero-inflated models in which individuals were either immobile with probability π or with probability $1 - \pi$ moved beyond a threshold distance according to a truncated standard distribution. We use a zero-inflated model with no threshold:

$$f_z(r) = \pi_z \delta(r) + (1 - \pi_z) f(r), \quad (1)$$

where $\delta(r)$ is the Dirac delta function, π_z is an additional parameter to be estimated, and the expected movement from model $f(r)$ is reduced by the factor $1 - \pi_z$. Zero-inflated models add flexibility to the otherwise simple and unimodal distributions of Table 2. For example, Paquet et al. (2020) compounded a movement kernel with Bernoulli 'site fidelity' that was set to zero for fledglings.

2.7 | Kernel properties

Each kernel type has a scale parameter, but values of that parameter are not directly comparable between types. For comparison, it is desirable to compute properties of the distribution of distance moved, such as the expected distance or the median (50th percentile) and 90th percentiles (Ergon & Gardner, 2014; Reidy et al., 2018). Theoretical values of these percentiles are provided by the distribution function (Table 2); realized percentiles will differ when settlement is limited to habitat patches (e.g., Reidy et al., 2018) or the distribution is truncated (see below). Quantiles of the distance moved are a monotonic function of the scale parameter for the single-parameter kernels BVN, BVE, BVC and RDE, so 95% confidence limits may be obtained by transforming the 95% limits for the scale parameter. The median distance is zero for zero-inflated models with $\pi_z \geq 0.5$ and hence, it is not useful for comparing such models.

Kernel tail weight (the relative probability of long-distance movement) has been assumed to predict the effect of emigration from a detector array on capture–recapture estimates of survival (Ergon & Gardner, 2014). We suggest the ratio of the 90th and 50th percentiles of distance moved as an index of tail weight in this context. This ratio, here denoted T_{90}, is constant for each of the single-parameter kernels RDE ($T_{90} \approx 3.32$), BVN ($T_{90} \approx 1.82$) and BVE ($T_{90} \approx 2.32$). The ratio otherwise depends inversely on the shape parameter β of each distribution (Figure 2). For BVT, $T_{90} \approx 5.74$ when $\beta = 0.5$, corresponding to bivariate Cauchy (BVC), and $T_{90} < 2$ when $\beta > 4.56$. Zero inflation increases the tail weight index for $\pi_z < 0.5$ and the index is not defined for $\pi_z \geq 0.5$.

The kernels also differ substantially in their shapes near zero ($r <$ median) (Figure 3). Many observations will relate to short-range

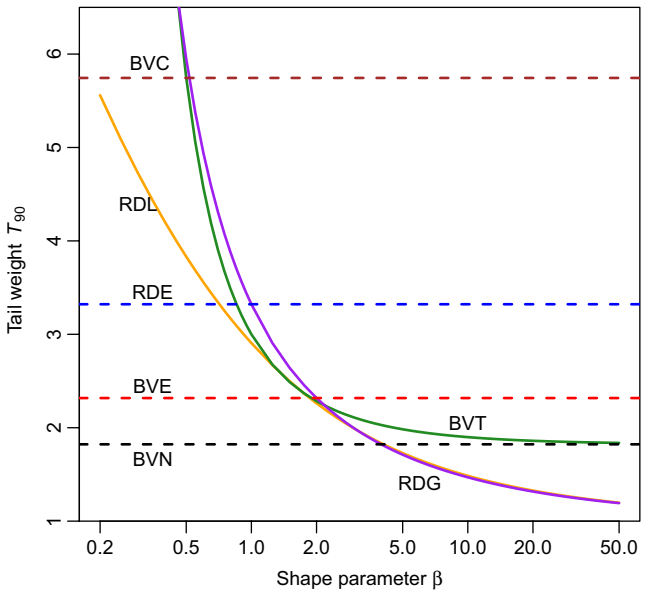

FIGURE 2 Relative tail weight of movement kernels (Table 2). An index of tail weight (T_{90} = ratio of 90th and 50th percentiles of distance moved) is plotted against the logarithm of the shape parameters β of the 2-parameter kernels BVT, RDL and RDG, and when constant (1-parameter kernels) as horizontal dashed lines.

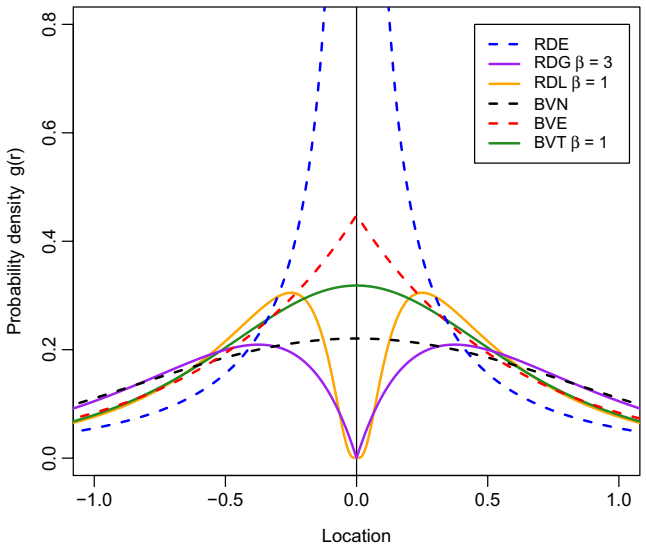

FIGURE 3 Cross-sections through the origin of 2-dimensional movement kernels $g(r)$. Kernels have the same median dispersal distance (1.0 units). One-parameter kernels (Table 2) are shown by a dashed line. Truncated function RDE is infinite at $r = 0$. RDG is zero at $r = 0$ for $\beta > 2$, as shown, but infinite at $r = 0$ for $\beta < 2$.

movements, which we expect to drive differences in fit among the candidate functions.

2.8 | Kernel discretization

Many SECR models are implemented in discrete space, including the likelihood-based applications of Glennie et al. (2019) and Efford and Schofield (2020). Activity centres are located at points on a square mesh, conceptually the centroids of grid cells. The movement model is then a discrete distribution, the probability of moving from a focal point to each other point on the mesh. Discrete kernels differ in their behaviour from continuous kernels, but the differences are subtle unless the median dispersal distance is only a few cells (Chesson & Lee, 2005) and apply primarily to the prediction of long-distance movement when kernel probabilites are compounded over multiple time steps (Chipperfield et al., 2011).

Pointwise probabilities may be approximated by evaluating the continuous 2-dimensional probability density at each mesh point and dividing by their sum. A more rigorous method is to compute each probability as the integral of the pdf across the enclosing grid cell, but this is slower and appears not to have been used in open SECR. Continuous distributions that are zero or infinite at the origin (the exponential, gamma or lognormal distributions of distance moved) pose a particular problem. The probability obtained by integrating the probability density over the origin cell is finite and positive. An approximation to the integrated value for the origin cell may be obtained from the cumulative distribution of distance moved ($F(r)$ in Table 2; Efford (2021)).

2.9 | Kernel truncation

Probability computations for maximum likelihood require repeated convolution of the kernel and the mesh, which can be time-consuming. Efford and Schofield (2020) made the problem more tractable by truncating the discretized kernel at a constant radius, effectively setting outer probabilities to zero, and renormalizing across the included points. This has negligible effect on the model if pointwise probabilities have declined to near zero at the chosen radius. The radius of truncation is an arbitrary component of the fitted model. The cumulative distribution of the continuous kernel function (Table 2) provides a check on the probability of exceeding the radius.

The expected movement for a kernel truncated at radius R is given by $E(r) = \int_0^R rf(r)\mathrm{d}r \,/\, \int_0^R f(r)\mathrm{d}r$ that may be computed by numerical integration of $f(r)$ in Table 2. The specific effect of kernel truncation is limited if all movement is truncated at the boundary of the habitat mask (see later section). There is no need in Bayesian model fitting to truncate the kernel as a Markov chain Monte Carlo (MCMC) update requires a single draw from the kernel distribution for each individual, relocating it anywhere in the habitat. The method of Glennie et al. (2019) also avoids truncation by applying a BVN kernel efficiently across the entire habitat, but it is not easily generalized to arbitrary kernels (R. Glennie, pers. comm.).

A discretized kernel can span many points, even if truncated. A 'sparse' kernel comprising points on eight 'spokes' at increments of $\pi/4$ radians can capture the essence of dispersal in open SECR (Efford, 2022b). The number of points in this configuration increases linearly with the truncation radius, rather than with its square, so quite large kernels become computationally feasible. Pointwise probabilities for $r > 0$ are weighted to restore the radial distribution

of probability, replacing $g(r)$ by $f(r) = 2\pi r g(r)$. The oblique axes have fewer cells, and these are upweighted by $\sqrt{2}$ to restore uniformity.

2.10 | Kernel-free methods

Movement may be modelled without specifying a probability kernel if each individual is relocated at random within a pre-defined region (the habitat mask or state space). This 'independent' or 'uncorrelated' model for successive locations has no estimated parameter and movements are truncated only at the outer boundary rather than at the edge of the discretized kernel. Independence is equivalent to specifying a uniform kernel of radius larger than the greatest dimension of the habitat mask, and truncating and renormalizing at the boundary (see below). Here, it is the 2-dimensional kernel $g(r)$ that is uniform, not the distribution of distances $f(r)$ (cf Ergon & Gardner, 2014). Average movement distances are directly buffer-dependent: for a circular area with diameter d the average distance is approximately $0.453d$, and for a square of side d the average is approximately $0.522d$ (e.g., Burgstaller & Pillichshammer, 2009). Average and median distances are easily obtained for discretized irregular areas (Appendix S4).

The 'independent' model may result in very biased estimates of survival (Ergon & Gardner, 2014; Gardner et al., 2018) and has not been shown to be a good fit to field data. In the simulations of Gardner et al. (2018) estimates of survival were unbiased only if the modelled region fortuitously matched the region used for data generation. The model is not neutral, but rather an extreme movement model with respect to what can be represented with a 2-dimensional kernel that declines monotonically from the point of origin (i.e., all models considered here except for gamma and log-normal distributions of radial distance; Figure 3). Independent relocation was applied by Augustine et al. (2020) to a capercaillie *Tetrao urogallus* dataset, with random relocation restricted to the current habitat patch. Using natural boundaries avoided some arbitrariness, and their survival estimates were likely unbiased by movement because the entire habitat was searched, but the movement model itself remains arbitrary (actual dispersal may have been on a scale smaller or larger than the patch).

A zero-inflated form of the 'independent' model has interesting properties. At each step an individual may remain where it is with probability π_z, or move to a uniform random location on the habitat mask. The probability π_z is an estimated parameter that varies movement between the extremes of independence with complete mixing ($\pi_z = 0$) and complete site attachment ($\pi_z = 1$). Any value of $\pi_z < 1$ leads to buffer dependence. The zero-inflation parameter provides some control over the average distance moved $(1 - \pi_z)\,E(r)$, where $E(r)$ is the expected value under independence. We consider the zero-inflated model in the case studies.

3 | SCALE OF SAMPLING

Movement modelling in open SECR can only be effective at separating emigration and mortality if sampling spans the full range of movements, or the distribution of movements beyond the surveyed region can be reliably inferred from shorter-range movements. Extrapolation from shorter range movements is inherently risky, as we demonstrate with a set of simulations. We considered movements arising from a mixture of two distributions, one compatible with the scale of sampling and one with larger scale, and evaluated fitted models in terms of their ability to recover the true survival probability.

The population was sampled with an 8×8 square array of detectors at spacing s on five sampling occasions. Initial locations were simulated uniformly in an arena $70s \times 70s$, and centres were allowed to move with no boundary. Movement was simulated via a two-part bivariate normal (BVN) mixture with equal weighting. The first mixture component had a scale comparable to that of the detector array ($E(d_1) = 3.5s$). We varied the scale of the second mixture component in multiples of the base scale ($E(d_2) = k\,E(d_1)$, $k = 1, \ldots, 5$, Figure 4a). Open SECR models were fitted using a buffer of width $7s$ and other standard assumptions (sparse discretized kernel radius $21s$; boundary rule 'truncate and renormalize'—see below). See Appendix S6 for details.

The effect of movement on survival estimates was largely eliminated when the scale of sampling roughly matched the scale of movement, and movements were homogeneous, i.e. $E(d_2)/E(d_1) = 1$ (Figure 4b). However, the method failed in the biologically realistic scenario that a fraction of individuals disperse to much greater distances, that is $E(d_2)/E(d_1) \gg 1$ (Figure 4b). Failure was uniform across light-tailed (BVN) and flexible (BVT) fitted distributions, and occurred even when the 2-class BVN model was fitted, the model from which data were generated.

4 | BOUNDARY EFFECTS

The activity centres of individuals detected in an open SECR study are initially within or near the detector array. If each individual follows a simple random walk then the centres of marked individuals tend over time to drift away from the array, and the area they occupy constantly expands.

Early open SECR models allowed the activity centres of marked individuals to drift indefinitely (Ergon & Gardner, 2014, Appendix S3; Schaub & Royle, 2014). These are described by their authors as spatial analogues of the non-spatial Cormack–Jolly–Seber method. The comparison is apt to the extent that they condition on first detection—a model of the spatial population is used only to model initial locations (Ergon & Gardner, 2014) or not at all if locations are observed without error (Schaub & Royle, 2014). We call these open SECR models 'unbounded' (Figure 5a). Unbounded models lack a state space in the sense of Royle et al. (2014). (The reference to a state space by Schaub and Royle (2014) appears to be an error).

The application of unbounded models is limited to the estimation of survival and movement parameters. For other parameters (recruitment, density or population rate of growth) a bounded region must be specified, at least with the current fitting methods that use

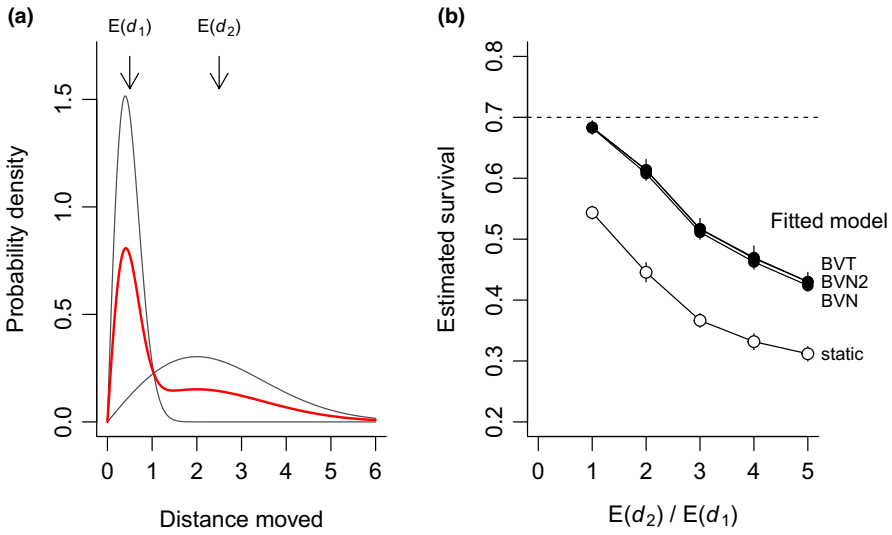

FIGURE 4 Effect of movement in relation to sampling scale on estimates of survival; simulated data with movements 50:50 mixture of bivariate normal distributions. (a) Distribution of distance moved (heavy red line) when second component had 5 times base distribution (thin lines; $E(d_1)$ = half grid width), and (b) survival estimates as function of relative scale of second component (bars show 95% CI). Fitted models: 'static' no movement, 'BVN' bivariate normal, 'BVN2' 2-class BVN mixture, 'BVT' bivariate *t* -distribution. Dashed line shows true survival probability.

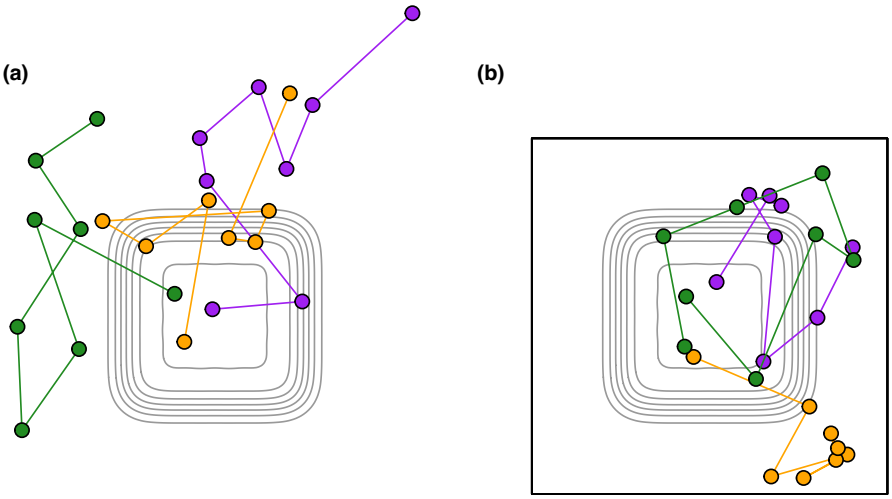

FIGURE 5 Movement paths of hypothetical individuals initially detected within a detector array, given (a) movement unbounded, or (b) movement kernel truncated at square boundary. Contours indicate declining detection probability on a central detector array. Enclosure increases the probability that emigrants later return to the zone of high detection probability, that is that emigration is temporary.

either data augmentation and MCMC or numerical integration. This raises the question of how to model movements so that modelled individuals remain within the model space; we call this the 'boundary rule' (Appendix S4).

A feasible and effective rule is to truncate each probability kernel at the boundary, and to renormalize the probabilities ('truncate and renormalize'). This is equivalent to repeatedly drawing locations from the kernel until one is found that lies within the boundary (i.e. rejection sampling), and is the rule stated or implied in the bounded Bayesian models in Table 1. Truncation introduces centripetal bias in the direction of movement that is greatest close to the boundary, and constrains the average realized movement (Appendix S4). In the limit, as the spatial scale of movement increases, realized distances match the independent, kernel-free model and are entirely buffer-dependent.

The Brownian motion algorithm of Glennie et al. (2019) generates long-range movements from multiple cell–cell steps. Its behaviour at the boundary is subtly different from 'truncate and renormalize' because animals encountering the boundary reorient their movement and continue (Pedersen et al., 2011, p. 1282). This is a plausible model for animal behaviour at a hard boundary, and such behaviour is amenable to field investigation that ultimately may lead to realistic open SECR models (McClintock et al., 2021). However, the outer boundary in open SECR is generally 'soft' (i.e., it does not correspond to any habitat feature), so there is no a priori reason to prefer this model over 'truncate and renormalize'.

5 | CASE STUDIES

We explored the issues of model selection and buffer dependence by analysing two datasets that we outline here and describe at greater length in Appendix S5. The ovenbird data are from a multi-species banding study over the 2005–2009 breeding seasons in eastern deciduous forest on the Patuxent Research Refuge, Maryland, USA (Dawson & Efford, 2009). Ovenbirds were mistnetted at 44 points spaced 30 m apart on a rectangular loop yielding 215 detections of 70 individuals. Tigers were monitored with automatic cameras over 10 years in the 644-km^2 Nagarahole reserve in the state of Karnataka, southern India (Karanth et al., 2006). We use the data analysed by Gardner et al. (2018) and published by Gardner et al. (2021). These comprise 343 detections of 75 tigers.

5.1 | Model selection

The choice of movement model in open SECR has tended to rest on a priori arguments (the desirability of a heavy tail) or ad hoc criteria such as convenience. Information theoretic criteria such as Akaike's information criterion (AIC) provide a straightforward basis for evaluating capture–recapture models and weighting them for model averaging. In this section, we demonstrate AIC model selection across a wide range of models for the ovenbird and tiger case studies. Buffer width was fixed initially at 800 m in the ovenbird models and 15 km in the tiger models.

Comparisons of movement models revealed both strong similarities and differences between the two studies (Table 3). The static and independent models carried negligible weight in either study. The bivariate normal BVN was also disfavoured in both studies. Two-parameter models were favoured and showed a strong peak at zero distance (Appendix S5). The fitted zero-inflated BVN and BVE kernels for ovenbirds were indistinguishable from the zero-inflated independent (uniform) model for the same reason. All ovenbird models with two movement parameters were rank-deficient, indicating that the movement scale parameter could not be estimated reliably. All tiger models were of full rank except for RDL, but the relative standard error (RSE) of movement parameters exceeded 1.0 or was not estimable for RDG and BVT (other RSE in range 0.07–0.66).

The model-averaged estimate of ovenbird survival (0.764, 95% CI 0.394–0.942) was imprecise, reflecting the spread of competitive models (Table 3, Appendix S5). The model-averaged estimate of tiger survival (0.785, 95% CI 0.691–0.862) was only slightly greater than previous estimates (Gardner et al., 2018; Karanth et al., 2006) and reasonably precise.

5.2 | Buffer dependence

The effect of buffer width on survival estimates was assessed empirically for the ovenbird and tiger case studies. The results depended upon the chosen movement model (Figure 6). The relationship between estimated survival and buffer width appeared to be asymptotic or nearly so in the tiger case: increase in buffer width beyond 15 km had negligible effect for most models except BVT. Ovenbird models, including BVT, also reached an asymptote of estimated survival with increasing buffer width. An exception for both studies was the zero-inflated independent model, for which estimated survival remained strongly dependent on buffer width across the ranges considered. This model was easily dismissed for tigers because of its poor fit, but in the ovenbird study it was competitive with other models causing the model-averaged estimate of ovenbird survival to depend on buffer width across the entire range (Figure 6). We conclude that the ovenbird data are consistent with a wide range of possible survival probabilities, and that movement and survival are confounded in the open SECR model. The tiger data are more promising, but there remains significant variation among movement models and a wide buffer is needed to escape buffer dependence.

6 | DISCUSSION

Movement models have appeared in several different forms in open-population spatial capture–recapture over its short history. Researchers have aimed to model dispersal without directional bias, except where settlement may depend on habitat covariates (e.g., Bischof et al., 2020). Circular kernels may be specified either as the

TABLE 3 Comparison of movement models for case-study datasets. AIC-best model emphasized. 'npm' number of parameters for movement kernel, 'logLik' maximized log likelihood, 'ΔAIC' difference in AIC from best model (bold), 'AICwt' AIC weight, '*E*(*d*)' average movement (km) (italicized estimates unreliable)

		Ovenbird				Tiger			
Model	npm	logLik	ΔAIC	AICwt	*E*(*d*)	logLik	ΔAIC	AICwt	*E*(*d*)
Static	0	−1,448.7	36.02	0.000	0.00	−1,408.8	23.89	0.000	0.00
RDE	1	−1,431.1	2.74	0.074	0.17	−1,400.1	8.45	0.004	0.81
RDG	2	−1,430.1	2.86	0.069	*0.07*	−1,395.7	1.68	0.119	*0.00*
RDL	2	−1,430.1	2.87	0.069	*0.06*	−1,395.9	2.08	0.097	*0.00*
BVN	1	−1,433.7	8.10	0.005	0.17	−1,400.8	9.83	0.002	1.27
BVE	1	−1,432.1	4.86	0.026	0.17	−1,400.3	8.96	0.003	1.11
BVT	2	−1,430.2	3.02	0.064	*0.15*	−1,395.9	2.09	0.097	*0.95*
RDEzi	2	−1,429.6	1.86	0.114	*0.18*	−1,395.3	1.00	0.167	0.69
BVNzi	2	−1,429.4	1.38	0.145	*0.21*	**−1,394.8**	**0.00**	**0.275**	**0.67**
BVEzi	2	−1,429.4	1.38	0.145	*0.21*	−1,395.1	0.55	0.209	0.73
IND	0	−1,465.2	69.06	0.000	0.91	−1,562.2	330.6	0.000	21.18
INDzi	1	**−1,429.7**	**0.00**	**0.289**	0.55	−1,398.1	4.55	0.028	3.28

Notes: 'static' no movement; RDE Exponential radial distance; RDG Gamma radial distance; BVN bivariate normal; BVE bivariate Laplace; BVT bivariate *t*; IND independent location within habitat mask; 'zi' suffix indicates zero-inflated.

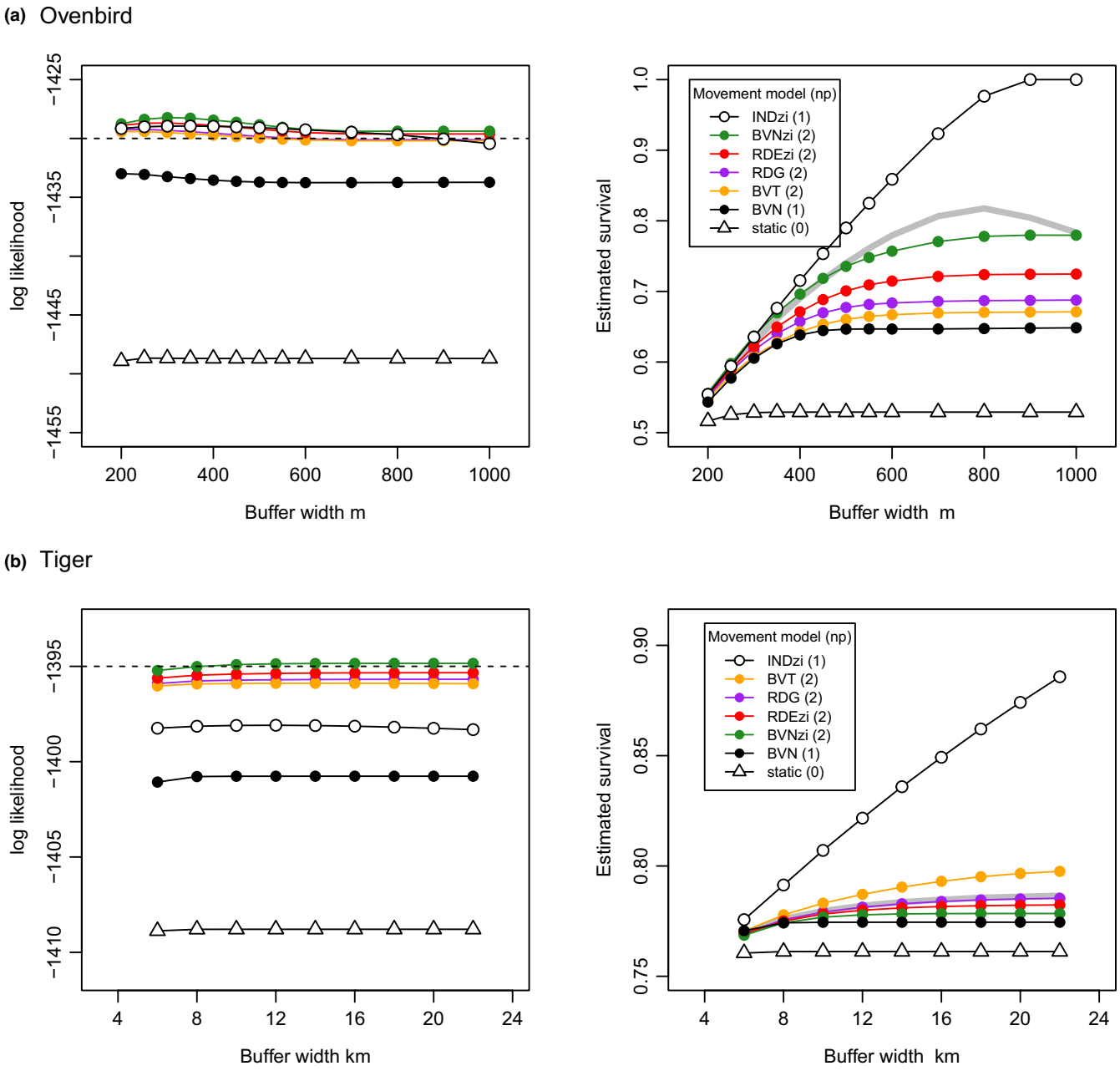

FIGURE 6 Empirical evaluation of buffer width for ovenbird and tiger datasets: seven movement models (Table 3) refitted with buffers of arbitrary width. Wide grey line shows survival estimates model-averaged using AIC weights. 'np' number of movement parameters.

joint, bivariate distribution of the displacement in *x*- and *y*-directions, or as the combined result of independent univariate distributions in polar coordinates (uniform angle, non-negative distance). These approaches are interchangeable. A third approach, to specify independent univariate distributions for the *x*- and *y*-coordinates, yields a circular distribution only in the special case of the normal distribution. We recommend this approach be avoided.

Open SECR models that included movement fit better than static models and gave reduced estimates of the scale of detection σ in all comparisons to date. Which movement model was chosen made virtually no difference to estimates of detection parameters (λ_0, σ) in our case studies, but it did affect estimates of survival and recruitment (Appendix S5). The popular BVN kernel performed poorly and is likely to lead to underestimation of survival.

Our problem is to choose among the more plausible movement models. Exhaustive comparison is not an option as the choices are many and not limited to those we considered. Instead, we suggest users compare 1-parameter models from across the spectrum of fixed tail weight (light, BVN; moderate BVE, RDE; heavy, BVC) or use the more flexible 2-parameter models (BVT, RDG, RDL, BVNzi, BVEzi, RDEzi). There was little to separate the flexible models in our case studies: kernels could be superficially different (Figure 3) while yielding very similar estimates of non-movement parameters, as the fitted shapes converged (Appendix S5). The flexible kernels

we considered are heavy-tailed only for small values of the shape parameter (Figure 2) so this should not be restricted to large values. Survival and recruitment estimates may be model-averaged to allow for uncertainty regarding the correct model.

A reviewer raised the possibility of confounding between the open SECR movement model and the detection model. We have implicitly assumed that each temporal sample includes spatial re-detections sufficient to fit the detection model, as in closed SECR. This requires either the robust design of Pollock (1982) or a detection process that allows multiple events in one sampling interval (automatic cameras or passive DNA sampling; Efford et al., 2009). Empirical trials lead us to speculate that, given this condition, the detection and movement models are not confounded.

Buffer dependence is a weakness in SECR models because buffer width is an arbitrary choice of the analyst. If survival estimates from an otherwise competitive model are not asymptotic with respect to buffer width then we infer that the model cannot be reliably estimated from the data, and estimates should not be reported. One warning sign is that the highly buffer-dependent zero-inflated independent model is competitive with respect to AIC, as in our ovenbird example. Difficulties in estimation of movement are a function of the data, and may reflect inadequate scale of sampling.

In closed SECR, the adequacy of any chosen buffer width for a specific detection function is readily checked post hoc by plotting its effect on the effective sampling area or an approximation (e.g., function 'esa.plot' in Efford (2022a)). Evaluating buffer-dependence in bounded open SECR models at present requires that each model is re-fitted for a range of buffer widths, which is time consuming. Further analysis of the relationship between survival estimates and buffer width may identify a family of curves that can be relied upon to extrapolate the asymptote or infer an adequate buffer width from trial fits.

Kernel-free 'independent' models are inherently buffer-dependent and can imply unrealistically large expected movement. These attributes explain their poor performance in the simulations of Gardner et al. (2018) and the low maximized likelihood in our examples. However, a zero-inflated independent model (INDzi) is useful heuristically and as a limiting case. Other zero-inflated models have a tendency to collapse to INDzi as indicated by a large value for the estimated scale of movement (Appendix S5). Large variance implies a nearly uniform distribution if movements are truncated at either the edge of the habitat mask or the edge of a discretized kernel. The inverse of the variance (precision) approaches zero, a boundary of the parameter space, which explains rank deficiency in the numerically fitted Hessian (Viallefont et al., 1999).

Ergon and Gardner (2014) stated clearly the potential limitations of open SECR for separating mortality and emigration:

> The accuracy of the survival estimates… is obviously contingent on a realistic model for dispersal away from the trapping array. We can only say something about the distribution of dispersal distances within the area covered by the trapping array, and if we fit the wrong weight of the dispersal distribution outside the trapping array, significant bias may result. It is obviously most important to account for dispersal when the study area is small relative to dispersal distances, but when this is the case, we have little information about the shape of the dispersal function.

Gilroy et al. (2012, p. 1515) had earlier highlighted the same issues. Inadequate scale of sampling is an insidious problem that may be impossible to diagnose from the data alone. The estimated scale of movement was quite small in the studies we reviewed (Appendix S2), but these estimates cannot be relied upon. Observed movements up to the scale of sampling may precisely match one distribution (e.g., BVN) and give no clue to the truncation of longer movements, as in our BVN-mixture example (Figure 4a). Open SECR cannot separate emigration from mortality without external information on the scale of dispersal. Prior biological knowledge may be used to ensure the study design is of sufficient scale, or the capture–recapture data may be augmented with data on dispersal from telemetry or sightings.

Ergon & Gardner (2014, p. 1334) raised the possibility that models may fit equally well but have very different tail weight, and hence lead to different estimates of survival, even when the scale of sampling is appropriate. Further investigation is needed, and it would be helpful to reproduce the effect in simulations. The scale of sampling was limited in our examples, and the data were somewhat weak and do not offer insight into this issue.

Our survey of movement kernels in open SECR has revealed many subtleties of parameterization and implementation. We call on authors to clearly distinguish among kernel types, including any truncation and boundary rules. Parameter constraints, including Bayesian priors, should be stated and explained. Comparison of studies is hindered when authors do not report numerical estimates of movement parameters, but merely provide a graph. Analysts should identify movement parameters that were estimated at a boundary of the parameter space (indicated by reduced rank of the hessian in ML). Given the variety of possible kernels it is desirable to report a standard description of movements, such as the expected distance $E(d)$ or the median and 90th percentiles (Ergon & Gardner, 2014; Reidy et al., 2018).

Movement models that apply a parametric distribution for distance moved are essentially phenomenological and give little insight into the movement process. Covariates such as age, sex and season may be included to elucidate the biology of dispersal and improve model fit. Conditioning settlement (and therefore distance moved) on local habitat covariates is another move towards greater biological realism.

There is wide scope for innovation in the modelling of movement in open SECR. Rather than an ever-expanding random walk, successive activity centres might be drawn from a stationary distribution representing a long-term (possibly multi-year) home range. A process such as the bivariate Ornstein-Uhlenbeck (Hooten et al., 2017) generates a stationary distribution with serial correlation that would be appropriate for samples spaced closely in time. We expect many

future SECR studies will have improved data resolution, both in space and time, that will allow the fitting of more flexible and realistic movement models (e.g., McClintock et al., 2021). It will be interesting to determine whether more realistic modelling of movement results in improved estimation of survival and recruitment. There may also be a trade-off in study design between investment in high resolution data and coverage of the target population.

The implications of artificially constraining the modelled population within a boundary require investigation. Enclosure inflates the probability of recapture and potentially distorts the spatial dynamics of the modelled population relative to the unbounded reality. The unbounded approach of Ergon and Gardner (2014) and Schaub and Royle (2014) may be preferable for studies of survival alone, and a maximum likelihood implementation would be welcome.

AUTHORS CONTRIBUTIONS

Murray G. Efford conceived the work and performed the simulations and analyses; Matthew R. Schofield contributed theoretical analysis. Writing was shared.

ACKNOWLEDGEMENTS

We thank Torbjørn Ergon, Beth Gardner, Michael Schaub, Richard Bischof, Grant Connette, Matthieu Paquet, and Richard Glennie for discussion and clarification of some points, and two anonymous reviewers for their helpful comments. Deanna Dawson led the mist-netting study and we thank her for making the data available. We acknowledge the use of New Zealand eScience Infrastructure (NeSI) high performance computing facilities URL https://www.nesi.org.nz.

CONFLICT OF INTEREST

We declare no conflict of interest.

PEER REVIEW

The peer review history for this article is available at https://publons.com/publon/10.1111/2041-210X.13947.

DATA AVAILABILITY STATEMENT

R code for the simulations on scale of sampling is available on Zenodo at https://doi.org/10.5281/zenodo.6622179 (Efford & Schofield, 2022; see also Appendix S6). The ovenbird data are available on Zenodo at https://doi.org/10.5281/zenodo.6622163 (Dawson & Efford, 2022). The tiger data are on Dryad Digital Repository at https://doi.org/10.5061/dryad.bcc2fqzd2 (Gardner et al., 2021).

ORCID

Murray G. Efford https://orcid.org/0000-0001-5231-5184
Matthew R. Schofield https://orcid.org/0000-0003-1481-2766

REFERENCES

Augustine, B., Kery, M., Marin, J. O., Mollet, P., Pasinelli, G., & Sutherland, C. (2020). Sex-specific population dynamics and demography of capercaillie (*Tetrao urogallus* L.) in a patchy environment. *Population Ecology*, *62*, 80–90.

Bischof, R., Brøseth, H., & Gimenez, O. (2016). Wildlife in a politically divided world: Insularism inflates estimates of brown bear abundance. *Conservation Letters*, *9*, 122–130.

Bischof, R., Milleret, C., Dupont, P., Chipperfield, J., Tourani, M., Ordiza, A., de Valpine, P., Turek, D., Royle, J. A., Gimenez, O., Flagstad, Ø., Åkesson, M., Svensson, L., Brøseth, H., & Kindbergh, J. (2020). Estimating and forecasting spatial population dynamics of apex predators using transnational genetic monitoring. *Proceedings of the National Academy of Sciences of the United States of America*, *117*, 30531–30538.

Borchers, D. L., & Efford, M. G. (2008). Spatially explicit maximum likelihood methods for capture–recapture studies. *Biometrics*, *64*, 377–385.

Burgstaller, B., & Pillichshammer, F. (2009). The average distance between two points. *Bulletin of the Australian Mathematical Society*, *80*, 353–359.

Chandler, R. B., & Clark, J. D. (2014). Spatially explicit integrated population models. *Methods in Ecology and Evolution*, *5*, 1351–1360.

Chandler, R. B., Hepinstall-Cymerman, J., Merker, S., Abernathy-Conners, H., & Cooper, R. J. (2018). Characterizing spatio-temporal variation in survival and recruitment with integrated population models. *Auk*, *135*, 409–426.

Chesson, P., & Lee, C. T. (2005). Families of discrete kernels for modeling dispersal. *Theoretical Population Biology*, *67*, 241–256.

Chipperfield, J. D., Holland, E. P., Dytham, C., Thomas, C. D., & Hovestadt, T. (2011). On the approximation of continuous dispersal kernels in discrete-space models. *Methods in Ecology and Evolution*, *2*, 668–681.

Clark, J. S., Silman, M., Kern, R., Macklin, E., & HilleRisLambers, J. (1999). Seed dispersal near and far: Patterns across temperate and tropical forests. *Ecology*, *80*, 1475–1494.

Clobert, J., Danchin, E., Dhondt, A. A., & Nichols, J. D. (2001). *Dispersal*. Oxford University Press.

Cousens, R., Dytham, C., & Law, R. (2008). *Dispersal in plants–A population perspective*. Oxford University Press.

Dawson, D. K., & Efford, M. G. (2009). Bird population density estimated from acoustic signals. *Journal of Applied Ecology*, *46*, 1201–1209.

Dawson, D. K., & Efford, M. G. (2022). Ovenbird mist-netting dataset. *Zenodo*, https://doi.org/10.5281/zenodo.6622163

Efford, M. G. (2021). *openCR: Open population capture–recapture models*. R package version 2.2.1. Retrieved from https://CRAN.R-project.org/package=openCR

Efford, M. G. (2022a). *secr: Spatially explicit capture-recapture models*. R package version 4.5.3. Retrieved from https://CRAN.R-project.org/package=secr

Efford, M. G. (2022b). Efficient discretization of movement kernels for spatiotemporal capture–recapture. *Journal of Agricultural, Biological and Environmental Statistics*, in press. https://doi.org/10.1007/s13253-022-00503-4

Efford, M. G., Dawson, D. K., & Borchers, D. L. (2009). Population density estimated from locations of animals on a passive detector array. *Ecology*, *90*, 2676–2682.

Efford, M. G., & Schofield, M. R. (2020). A spatial open-population capture–recapture model. *Biometrics*, *76*, 392–402.

Efford, M. G., & Schofield, M. R. (2022). R code for simulating the effect of spatial scale in open population capture–recapture sampling. *Zenodo*, https://doi.org/10.5281/zenodo.6622179

Ergon, T., & Gardner, B. (2014). Separating mortality and emigration: Modelling space use, dispersal and survival with robust-design spatial capture–recapture data. *Methods in Ecology and Evolution*, *5*, 1327–1336.

Fujiwara, M., Anderson, K. E., Neubert, M. G., & Caswell, H. (2006). On the estimation of dispersal kernels from individual mark–recapture data. *Environmental and Ecological Statistics*, *13*, 183–197.

Gardner, B., Sollmann, R., Kumar, N. S., Jathanna, D., & Karanth, K. U. (2018). State space and movement specification in open population spatial capture–recapture models. *Ecology and Evolution*, *8*, 10336–10344.

Gardner, B., Sollmann, R., Kumar, N. S., Jathanna, D., & Karanth, K. U. (2021). Ten-year camera-trap dataset of tigers in India. *Dryad Digital Repository*, https://doi.org/10.5061/dryad.bcc2fqzd2

Gardner, B. J., Reppucci, J., Lucherini, M., & Royle, J. A. (2010). Spatially-explicit inference for open populations: Estimating demographic parameters from camera-trap studies. *Ecology*, *91*, 3376–3383.

Gilroy, J. J., Virzi, T., Boulton, R. L., & Lockwood, J. L. (2012). A new approach to the 'apparent survival' problem: Estimating true survival rates from mark–recapture studies. *Ecology*, *93*, 1509–1516.

Glennie, R., Borchers, D. L., Murchie, M., Harmsen, B. J., & Foster, R. J. (2019). Open population maximum likelihood spatial capture–recapture. *Biometrics*, *75*, 1345–1355.

Honeycutt, R. K., Garwood, J. M., Lowe, W. H., & Hossack, B. R. (2019). Spatial capture–recapture reveals age- and sex-specific survival and movement in stream amphibians. *Oecologia*, *190*, 821–833.

Hooten, M. B., Johnson, D. S., McClintock, B. T., & Morales, J. M. (2017). *Animal movement: Statistical models for telemetry data*. CRC Press.

Karanth, K. U., Nichols, J. D., Kumar, N. S., & Hines, J. E. (2006). Assessing tiger population dynamics using photographic capture–recapture sampling. *Ecology*, *87*, 2925–2937.

Kendall, W. L., Nichols, J. D., & Hines, J. E. (1997). Estimating temporary emigration using capture–recapture data with Pollock's robust design. *Ecology*, *78*, 563–578.

Kotz, S., Kozubowski, T. J., & Podgörski, K. (2001). *The Laplace distribution and generalizations: A revisit with applications to communications, economics, engineering, and finance*. Birkhäuser.

Lebreton, J. D., Burnham, K. P., Clobert, J., & Anderson, D. R. (1992). Modeling survival and testing biological hypotheses using marked animals—A unified approach with case-studies. *Ecological Monographs*, *62*, 67–118.

Lebreton, J. D., Nichols, J. D., Barker, R. J., Pradel, R., & Spendelow, J. A. (2009). Modeling individual animal histories with multistate capture–recapture models. *Advances in Ecological Research*, *41*, 87–173.

McClintock, B. T., Abrahms, B., Chandler, R. B., Conn, P. B., Converse, S. J., Emmet, R. L., Gardner, B., Hostetter, N. J., & Johnson, D. S. (2021). An integrated path for spatial capture–recapture and animal movement modeling. *Ecology*, e03473. https://doi.org/10.1002/ecy.3473

McDonald, T. L., Hornsby, F. E., Speakman, T. R., Zolman, E. S., Mullin, K. D., Sinclair, C., Rosel, P. E., Thomas, L., & Schwacke, L. H. (2017). Survival, density, and abundance of common bottlenose dolphins in Barataria Bay (USA) following the *Deepwater Horizon* oil spill. *Endangered Species Research*, *33*, 193–209.

Milleret, C., Bischof, R., Dupont, P., Brøseth, H., Odden, J., & Mattisson, J. (2021). GPS collars have an apparent positive effect on the survival of a large carnivore. *Biology Letters*, *17*, 20210128.

Milleret, C., Dupont, P., Chipperfield, J., Turek, D., Brøseth, H., Gimenez, O., de Valpine, P., & Bischof, R. (2020). Estimating abundance with interruptions in data collection using open population spatial capture–recapture models. *Ecosphere*, *11*(7), e03172.

Muñoz, D. J., Miller, D. A. W., Sutherland, C., & Grant, E. H. C. (2016). Using spatial capture–recapture to elucidate population processes and space-use in herpetological studies. *Journal of Herpetology*, *50*, 570–581.

Nathan, R., Klein, E., Robledo-Arnuncio, J. J., & Revilla, E. (2012). Dispersal kernels: Review. In J. Clobert, et al. (Eds.), *Dispersal ecology and evolution* (pp. 187–210). Oxford University Press.

Paquet, M., Arlt, D., Knape, J., Low, M., Forslund, P., & Pärt, T. (2020). Why we should care about movements: Using spatially explicit integrated population models to assess habitat source–sink dynamics. *Journal of Animal Ecology*, *89*, 2922–2933.

Pedersen, M. W., Patterson, T. A., Thygesen, U. H., & Madsen, H. (2011). Estimating animal behavior and residency from movement data. *Oikos*, *120*, 1281–1290.

Pollock, K. H. (1982). A capture–recapture design robust to unequal probability of capture. *Journal of Wildlife Management*, *46*, 752–757.

Raabe, J. K., Gardner, B., & Hightower, J. E. (2014). A spatial capture–recapture model to estimate fish survival and location from linear continuous monitoring arrays. *Canadian Journal of Fisheries and Aquatic Sciences*, *71*, 120–130.

Reidy, J. L., Thompson, F. R., III, Connette, G. M., & O'Donnell, L. (2018). Demographic rates of Golden-cheeked Warblers in an urbanizing woodland preserve. *Condor*, *120*, 249–264.

Royle, J. A., Chandler, R. B., Sollmann, R., & Gardner, B. (2014). *Spatial capture–recapture*. Academic Press.

Satter, C. B., Augustine, B. C., Harmsen, B. J., Foster, R. J., & Kelly, M. J. (2019). Sex-specific population dynamics of ocelots in Belize using open population spatial capture–recapture. *Ecosphere*, *10*(7), e02792.

Schaub, M., & Royle, J. A. (2014). Estimating true instead of apparent survival using spatial Cormack–Jolly–Seber models. *Methods in Ecology and Evolution*, *5*, 1316–1326.

Van Houtan, K. S., Pimm, S. L., Halley, J. M., Bierregaard, R. O., Jr., & Lovejoy, T. E. (2007). Dispersal of Amazonian birds in continuous and fragmented forest. *Ecology Letters*, *10*, 219–229.

Viallefont, A., Lebreton, J.-D., Reboulet, A.-M., & Gory, G. (1999). Parameter identifiability and model selection in capture–recapture models: A numerical approach. *Biometrical Journal*, *40*, 313–325.

Whittington, J., & Sawaya, M. A. (2015). A comparison of grizzly bear demographic parameters estimated from non-spatial and spatial open population capture–recapture models. *PLoS ONE*, *10*(7), e0134446.

SUPPORTING INFORMATION

Additional supporting information can be found online in the Supporting Information section at the end of this article.

How to cite this article: Efford, M. G., & Schofield, M. R. (2022). A review of movement models in open population capture–recapture. *Methods in Ecology and Evolution*, *13*, 2106–2118. https://doi.org/10.1111/2041-210X.13947